Kinematic and thermal properties of a large-amplitude wave in the westerlies

By C. W. NEWTON, *U. S. Weather Bureau* and E. PALMÉN, *Academy of Finland*

(Manuscript received January 8, 1963)

ABSTRACT

The characteristics of a large-amplitude long wave, with superimposed short-wave disturbances, are described with emphasis on the deviations between the real and geostrophic winds, and between the corresponding vorticity fields.

In the long-wave trough and ridge, the maximum wind speed differed from the geostrophic wind by a factor of about two. Correspondingly large differences were observed between the thermal shear and the vertical shear of the real wind. Consistent with this, the slope of the polar front was much steeper in the trough, and shallower in the ridge, than is indicated by Margules' formula for straight flow. The vertical shear was also influenced by the change of trajectory curvature with height, which is shown to be systematically related in part to the vertical motion field.

The regions of strongest divergence and convergence in the upper troposphere lay very nearly on the jet-stream axis, and local maximum values were an order of magnitude larger than the mean divergence over the region between trough and ridge of the long wave.

Kinematically computed vertical motions indicate descent west and ascent east of the trough, in the warm air; in the cold air mass, however, there was ascent west and descent east of the trough line. The differential adiabatic heating or cooling associated with this distribution of vertical motions contributes to strengthening of the horizontal temperature gradient in air approaching the trough, and a weakening in the air streaming eastward from the trough. The indicated redistributions of potential energy are qualitatively in accord with kinetic energy variations along the current, on the west and east sides of the trough where marked deceleration and acceleration are observed in the upper troposphere.

1. Introduction

The general aspects of the three-dimensional fields of motion in atmospheric waves are well known, from theoretical and empirical studies by BJERKNES (1937), ROSSBY (1942), BJERKNES and HOLMBOE (1944), SUTCLIFFE (1947), FLEAGLE (1947), PALMÉN (1951), RIEHL and COLLABORATORS (1954), PETTERSSEN (1955), and other investigators. In this paper, we attempt to extend these results, by drawing attention to some of the properties of a large-amplitude long-wave system which are perhaps not so widely appreciated.

In particular, the great curvatures associated with large-amplitude waves, in combination with strong upper winds, give rise to centripetal accelerations which are large in proportion to the pressure-gradient and Coriolis accelerations. The variations of centripetal acceleration with height, associated both with the change of wind speed and of curvature with height, have important influences on the relationship between the vertical shear and the solenoid field. One of our objectives will be to demonstrate the very considerable differences in the structures of the wind and temperature fields in troughs and ridges, associated with these influences.

In addition, we will examine the vertical motion field and the fields of real and geostrophic vorticity associated with the long wave and the disturbances. Finally, a simple analysis will be carried out, to show a general relationship between the contour pattern and the three-dimensional trajectories in the middle troposphere.

2. Synoptic situation on December 12, 1957

A strong outbreak of very cold polar air occurred on December 11 to 12 over the central

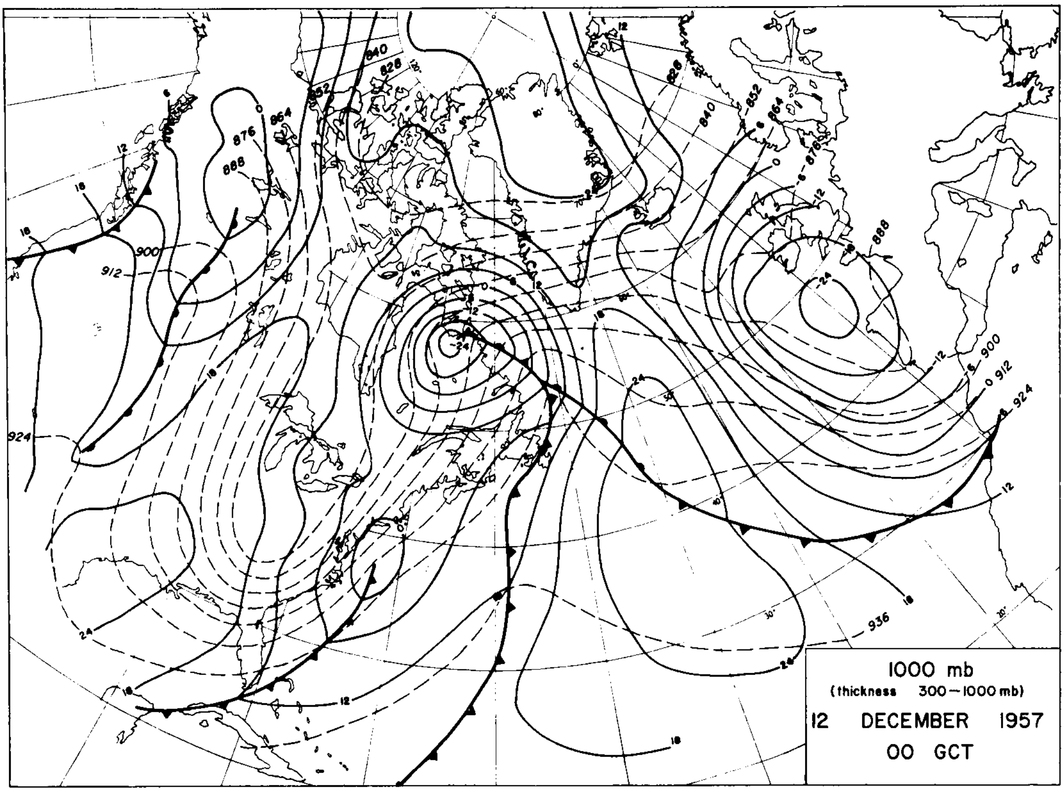

Fig. 1. 1000-mb contours (solid lines, heights in tens of meters), and thickness of the 300- to 1000-mb layer (dashed lines), 00 GMT December 12, 1957. Thickness interval (120 m) corresponds to layer-mean temperature difference of about 3°C.

and eastern parts of the United States. At 00 GMT December 12, the cold front had already passed the east coast and lay just south of Miami and on the north coast of Cuba. Prior to this fresh cold outbreak there had some days before been an earlier cold outbreak. The cold front of this previous cold mass could still be seen on the surface map (Fig. 1) over the Atlantic Ocean, extending southward and southwestward from the deep cyclone over Labrador. The older cold air mass was rapidly being transformed into a relatively warm mass, due to the combined effects of adiabatic heating due to subsidence, and to a strong transfer of heat from the warm ocean. Off the east coast of the United States, a new cyclonic disturbance was developing.

The structure of the atmosphere in a vertical cross section along the parallel 35°N at the synoptic times 12 GMT December 11 and 00 GMT December 12 has the character of the schematic Fig. 2, where the polar front is indicated by a solid line for the earlier time, and a dashed line for the later.

The schematic shape of the polar front serves

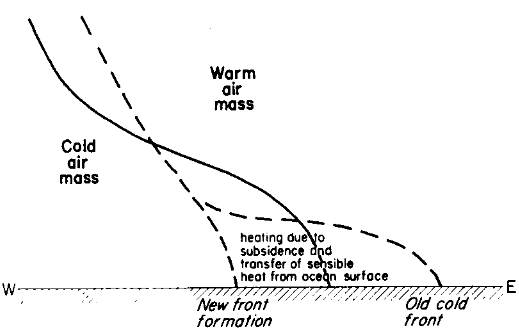

Fig. 2. Schematic illustration of the formation of a polar front in the surface layers, off the east coast of the U. S.

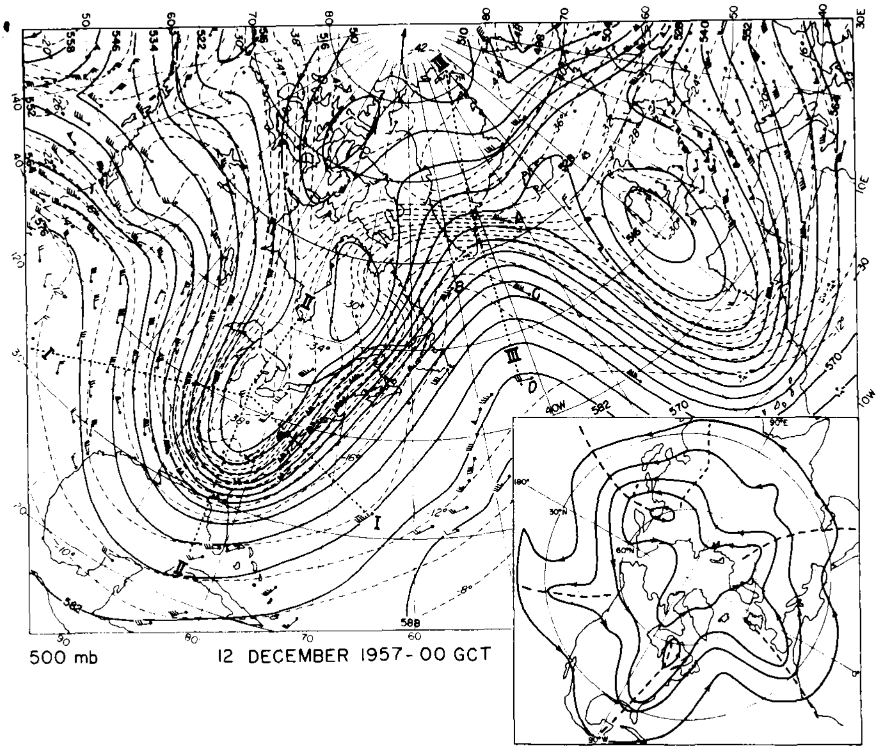

Fig. 3. Contours (solid lines in tens of meters) and isotherms (dashed lines, deg. C) at 500 mb, 00 GMT December 12, 1957. Inset shows hemispheric wave pattern, contours at 240-m interval; outer contour is 5820 m.

to indicate the subsidence of the cold-air wedge and the formation of a new surface front, with old heated polar air to the east and fresh polar air to the west of the vertical through the point where the upper front shows a rapid steepening in slope. The surface front forms on a line representing the vertical projection of the upper line along which this change of slope occurs. The new front rapidly becomes the main surface front, and already after 12 hours it can be treated as a surface polar front in spite of the prehistory. Hence the disturbance forming northeast of Hatteras can be considered a wave cyclone of the polar front.

To the west of the cold surface ridge over the central parts of the United States, another cyclonic disturbance was advancing eastward over the Rocky Mountains. It was associated with a minor disturbance of the strong upper flow of relatively warm middle-latitude air; but, as usual, its structure on the surface map was diffuse in this region partly due to the orography.

At the 500-mb level (Fig. 3), the polar front was very well marked by a bundle of isotherms connected with a very intense major cold trough. This band extended from Alaska to the southeastern United States, thence northeastward along the Atlantic coast and through the warm upper ridge over southern Greenland. Its further extension over the eastern Atlantic Ocean is less clear, but still relatively well marked in the thermal field.

The deep upper trough over the United States was one of the five major troughs that could be seen on the 500-mb chart for the Northern Hemisphere at this time. This trough, and the downstream ridge at longitude 40° W, are the most impressive features on the chart, considering both the thermal structure and wind field. This wave system has therefore been selected as a good example for a detailed synoptic examination. The overall thermal pattern, in relation to the flow pattern, is quite similar to that in other hemispheric analyses which have been

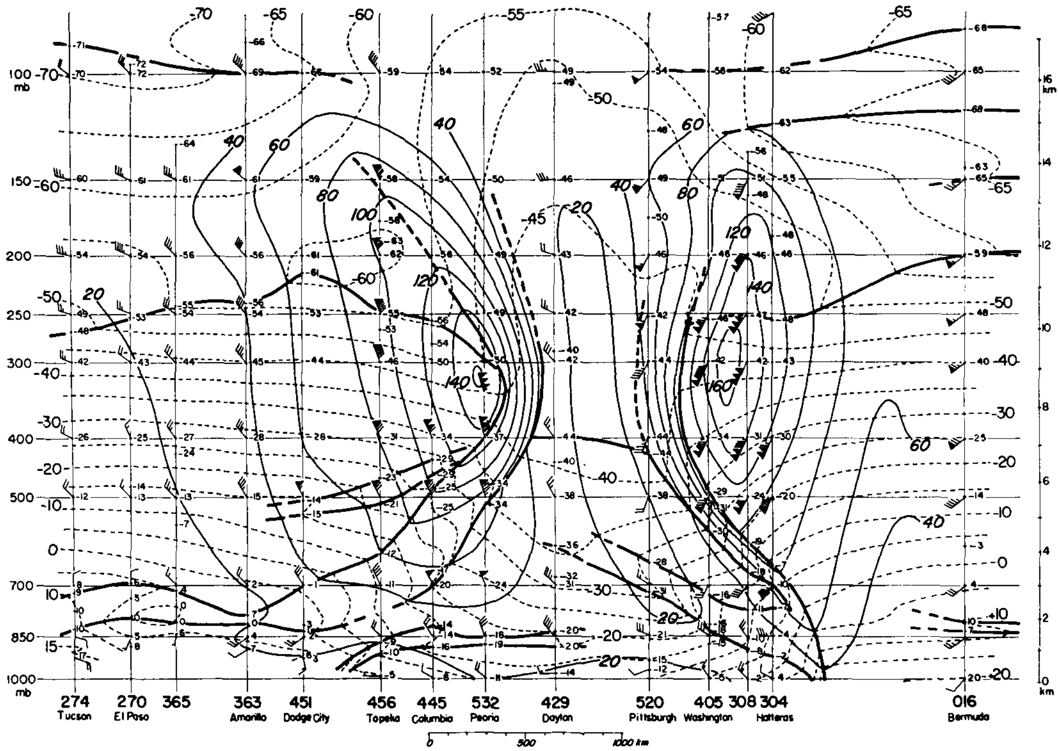

Fig. 4*a*. Cross section along line I in Fig. 3. Heavy lines are frontal boundaries and tropopauses, solid thin lines, isotachs (knots); dashed lines, isotherms (deg. C).

published (see, for example, BRADBURY and PALMÉN, 1953).

3. Structure of the trough and ridge

Three vertical cross sections along the lines I, II and III in Fig. 3 will be shown. These illustrate the distribution of temperature, potential temperature and wind velocity, the wind direction in the upper levels being approximately normal to the sections. Fig. 4, a section along the broken line (I–I) running SW–NE–SE in Fig. 3, extends across the NW current on the west side of the trough and across the SW current on the east side.

This cross section shows the characteristic structure of an intense trough with a strong jet, of maximum velocity about 160 knots around the 300-mb level, with the characteristic breaks between the tropopauses of the warm air and the polar air. The polar tropopause was at the low altitude of around 400 mb, but from 600 to 400 mb the vertical stability was strong, almost corresponding to stratospheric conditions, over Dayton in the central part of the cold tongue. This is probably the result of vertical shrinking in the upper troposphere in the polar air, which results in formation of a "false" tropopause around the 600-mb level. The tropical tropopause can be seen at very high altitudes, around 100 mb on the west side and 120 mb on the east side. At 300–350 mb, the difference in temperature between the polar air and the middle-latitude air vanishes. Here the frontal layer is characterized by strong horizontal wind shear, but no horizontal temperature gradient, as is characteristic of the transition zone between stratosphere and troposphere. The frontal analysis has been extended somewhat into the lower stratosphere where the frontal layer (embracing the zone of strongest cyclonic shear and temperature gradient) gradually vanishes upwards. The polar air, both in the troposphere and the stratosphere, is as usual characterized by relatively weak winds. In the lower part of the troposphere the frontal layer is characteri-

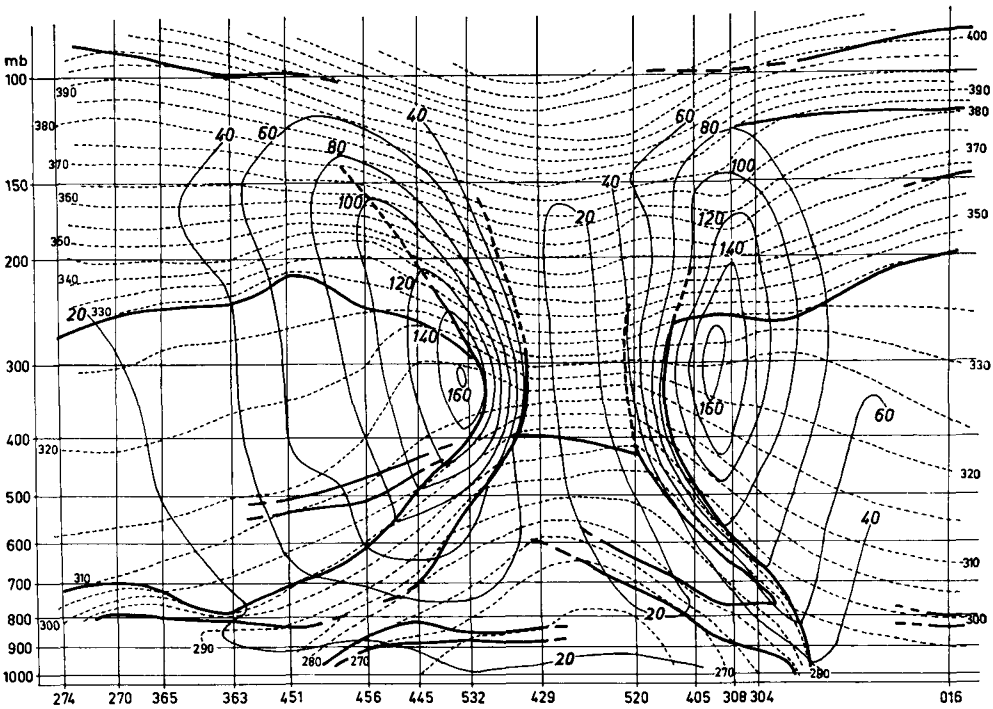

Fig. 4*b*. Same cross section as in Fig. 4*a*, but darked lines are here isentropes (deg. K).

zed by change in the wind shear across the frontal boundaries, but not necessarily by a change in the wind velocity across the whole front. On the west side the velocity is really higher on the cold side than on the warm side, showing an average anticyclonic wind shear in the frontal zone. In the upper troposphere, above about 600 mb, the fronts show strong cyclonic wind shear.

In the meridional cross section approximately at the trough (Fig. 5), the frontal layer is somewhat diffuse (except in the lower portion) but has a considerable depth. Here the break between the polar tropopause and the middle-latitude tropopause is extreme. The polar tropopause sinks down to below the 500-mb surface just north of the front. The tropical tropopause, having a double structure, lies around 100 mb as in cross section I. Figure 5 shows an extreme case where the tropical tropopause and the polar tropopause have been brought to almost the same latitude.

The wind speed in the jet stream is weaker in cross section II than on either side of section I (Fig. 4), indicating a strong deceleration on the west side of the trough line and strong acceleration on the east side. This conclusion is valid since the wind speed in the jet was much greater than the speed of progression of the trough, so that the air on the west side streams through to the east side of the trough.

In cross section III along the upper ridge at about longitude 40° W (Fig. 6), the frontal structure is very clear, both considering the wind field as shown by the isotachs, and the thermal field as shown by isotherms and isentropes. The 300-mb velocity of the jet stream is somewhat over 120 knots, or about the same as on the trough line. The difference in tropopause height is small, the polar tropopause being high. The warm-air tropopause has a double structure over Ships "B", "C", and "D". Both air masses in the upper half of the troposphere are almost barotropic, and the meridional baroclinity is

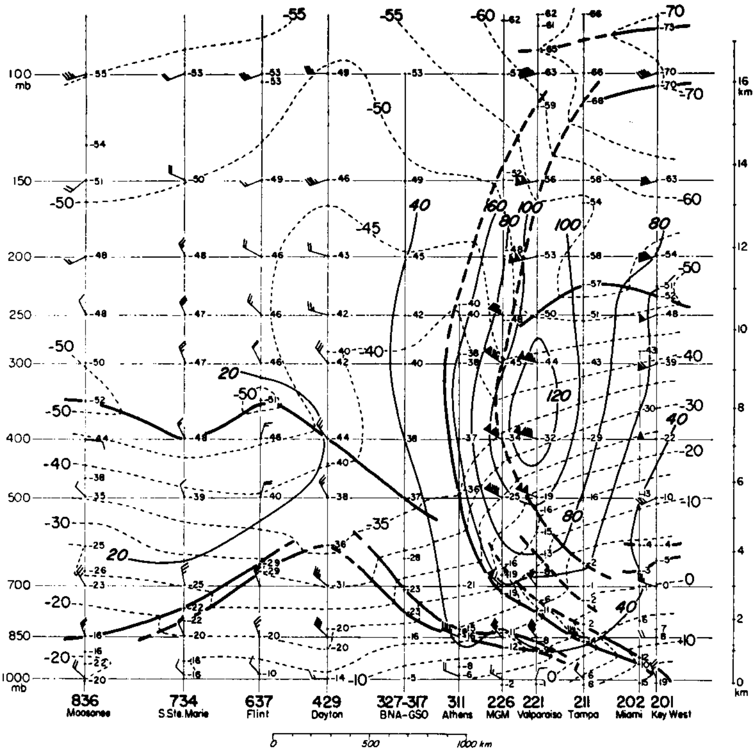

Fig. 5*a*. Cross section along line II in trough of Fig. 3. Dashed lines are isotherms.

almost totally concentrated in the front, the structure of which is shown very clearly by five different soundings near the ridge line.[1]

4. Comparison of real and geostrophic wind speeds

The relationship between wind velocity and normal pressure gradient in the trough and ridge can be computed from the equation

$$V = V_g - \frac{KV^2}{f}, \tag{1}$$

where V is the observed wind, V_g the geostrophic wind, and K (here, and where it appears later without a subscript)the trajectory curvature. In this case, K can approximately be computed from Blaton's formula

$$K = K_s\left(1 - \frac{c}{V}\right), \tag{2}$$

where K_s is the curvature of a streamline and c denotes the celerity of the system (the eastward movement of the trough or ridge line). The streamline curvature, measured from isogon analyses, is the geodesic curvature (PLATZMAN, 1947)

$$K_s = \partial\beta/\partial s + (\cos\beta \tan\Phi)/a, \tag{3}$$

where β is the wind direction (radians) measured counterclockwise from east, s is distance along a streamline, a the earth's radius, and Φ the latitude.

In Fig. 7 the curves marked Z show the height of the 300-mb surface along the meridians of the trough and ridge lines. The dashed curves marked V_{g1} represent the geostrophic velocity computed from the Z-curves, whereas the curves marked V give the distribution of actual wind speed, taken from an isotach analysis at the 300-mb surface, based on observed winds.

[1] In Fig. 6, composite soundings are represented for the pairs of stations 220 and 360, and weather ships "B" and "C". In each case, one of the stations lies some distance east, and the other to the west, of the ridge line but the individual soundings of each pair are very similar to each other.

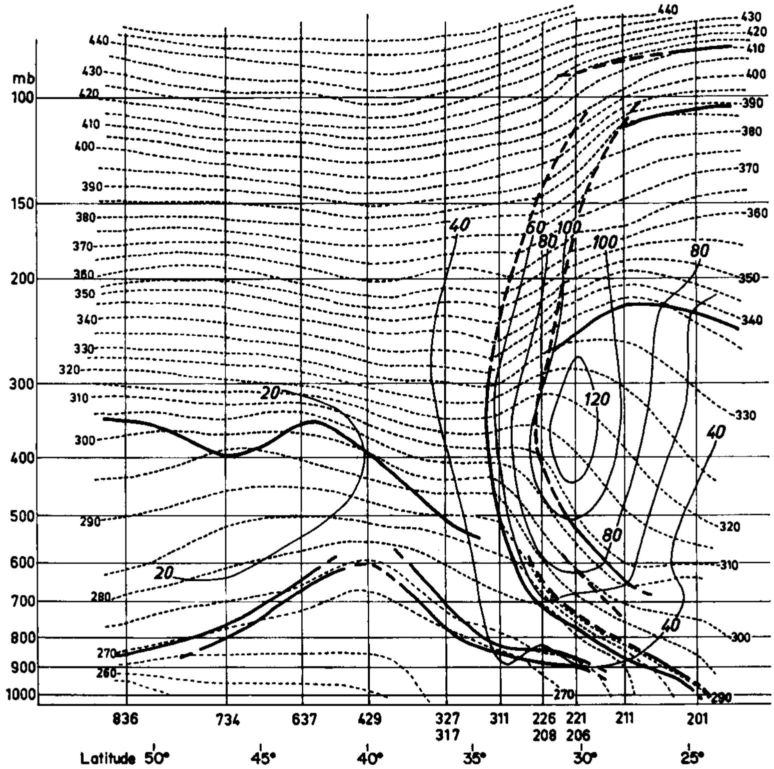

Fig. 5*b*. Same cross section as in Fig. 5*a*. Dashed lines are here isentropes.

For comparison with V_{g1}, curves V_{g2} are shown, which give the geostrophic wind computed without direct recourse to the contour analysis, by inserting observed values of V and K into eq. (1). The differences between the independently-derived curves V_{g1} and V_{g2} can be accounted for by relatively small uncertainties in the analyzed contour and/or wind-velocity fields.

Fig. 7 shows the strong effect of the curvature. At the trough line the maximum observed wind at the 300-mb level is only 60 m/sec whereas the geostrophic wind computed from the contours of the 300-mb surface amounts to 118 m/sec, or double the observed wind, at the corresponding latitude. At the ridge line the observed wind maximum of 66 m/sec corresponds to a geostrophic wind of about 38 m/sec. As will be seen later, these deviations between real and geostrophic wind, when combined with truncation errors, result in a very considerable distortion of the geostrophic from the real vorticity distribution, particularly near the level of strongest wind.

A comparison of Figs. 5 and 6 reveals that the overall airmass contrasts were essentially the same in the neighborhood of trough and ridge. However, the trough was characterized by a strong baroclinic field extending through a very deep layer, while the strong baroclinity at the ridge line was confined essentially to a relatively shallow frontal layer.

In the upper troposphere the slope of the front was much larger in trough than in ridge. This difference may be seen to be primarily associated with difference in curvature. Margules' formula for the slope of a front, when modified (Exner, 1925) to take curvature into account, states that

$$\tan \psi = \frac{(f + 2KV)\,T}{g} \frac{\delta V}{\delta T}. \tag{4}$$

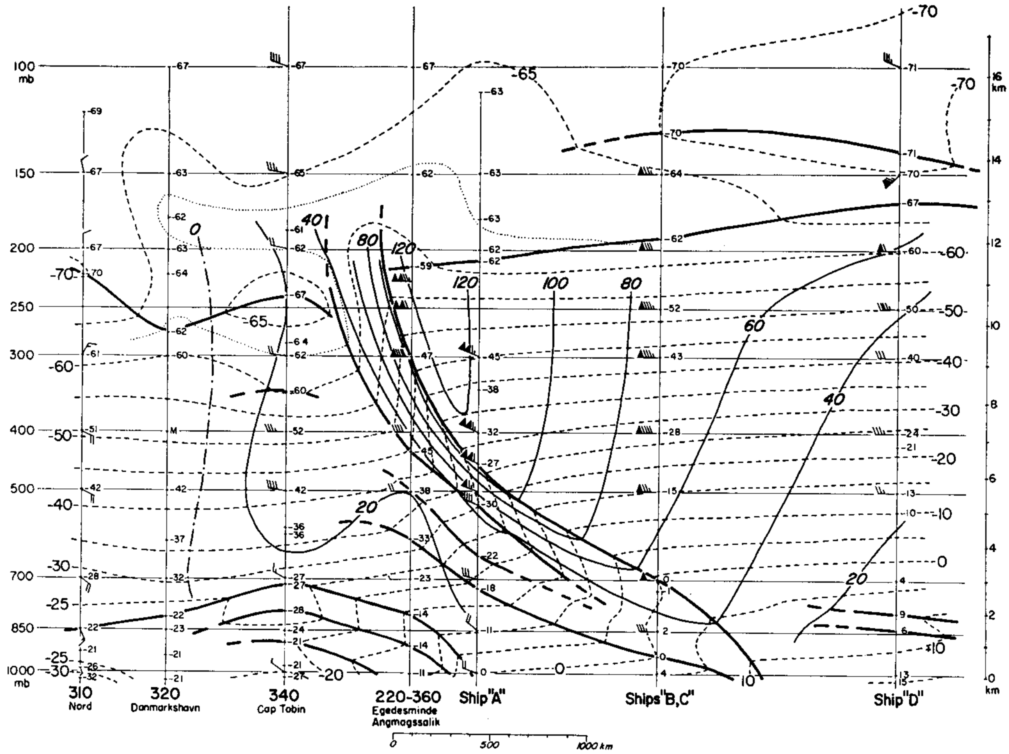

Fig. 6*a*. Cross section along line III in ridge of Fig. 3. Isotachs were taken from isobaric charts along this line, and do not necessarily agree with plotted winds which in some cases correspond to stations some distance east or west of section. Dashed lines are isotherms.

This expression, although derived for a discontinuity surface of zero order, is applicable to a frontal layer of finite width provided that the difference in gradient wind speed δV across the frontal layer is measured in the vertical and the temperature difference δT along an isobaric surface. With good approximation, δV can be replaced with the difference in observed wind speed parallel to the frontal intersection with an isobaric surface. In Figs. 5 and 6, δT is seen to be nearly the same in the two locations, of the order 15°C at, for instance, the 500-mb surface. The wind difference δV through the strong baroclinic layer is likewise nearly the same, about 60 kt.

In the latitude of strongest wind, f was about $0.6 \times 10^{-4}\text{sec}^{-1}$ greater in ridge than in trough, so that the Coriolis parameter would itself contribute toward a steeper slope in high latitudes. However, the variation of curvature overcompensates this variation of Coriolis parameter. Adopting the value of 1500 km for the radius of curvature of a trajectory in both ridge and trough, and a wind speed of 40 m/sec, $|2KV| = 0.53 \times 10^{-4}\text{sec}^{-1}$. The curvature term would thus be $1.06 \times 10^{-4}\text{sec}^{-1}$ larger in trough than in ridge. The quantity $(f + 2KV)$ would, correspondingly, be almost twice as large in trough as in ridge. From the cross sections, the frontal slope at 500 mb is estimated to be 1.1×10^{-2} in the trough, and 0.5×10^{-2} in the ridge, in good agreement with the theoretical values of the difference in slope.

Between the trough and ridge in the cross section of Fig. 4 where the curvature was small, the temperature difference amounted to about 10°C and the wind difference to about 60 kt. Considering f to be $0.9 \times 10^{-4}\text{sec}^{-1}$ at this latitude, the slope of the front would be 0.7×10^{-2} according to eq. (4). This approximately corresponds to the slope of about 0.75×10^{-2} measured from Fig. 4. Thus the variation in frontal slope from the trough to the ridge is in close accord with the simple Margules' formula applied for a frontal layer of finite width, but only if the curvature is taken into account.

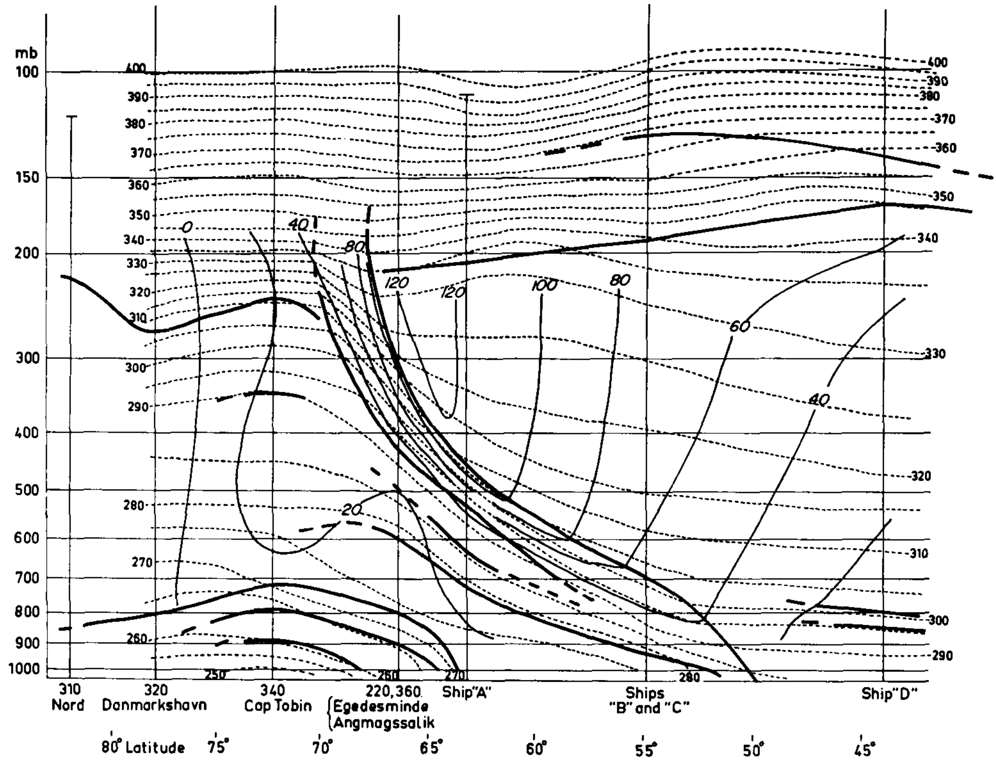

Fig. 6*b*. Same cross section as in Fig. 6*a*. Dashed lines are here isentropes.

5. Vertical wind shear in comparison with thermal wind

The presence of strong baroclinity throughout the troposphere in the trough, and its virtual confinement to the frontal layer in the ridge, is reflected in the character of the wind profiles in the vertical. Fig. 8 shows the distribution of wind velocity and temperature at Ship "A" near the ridge. In the well marked frontal layer between 525 and 450 mb the wind velocity increased by 70 kt (or 80 kt if we put the upper boundary of the layer at 440 mb). This is equivalent to a wind increase of about 33 m/sec per km or a vertical wind shear of $33 \times 10^{-3}\,\mathrm{sec}^{-1}$. By using the thermal wind equation

$$\frac{\partial V_g}{\partial z} = -\frac{g}{fT}\left(\frac{\partial T}{\partial n}\right)_p,$$

the vertical shear of V_g was computed to be $18 \times 10^{-3}\,\mathrm{sec}^{-1}$.

Taking the curvature into account (FORSYTHE, 1945), the vertical wind shear is determined by

$$\frac{\partial V}{\partial z} = \frac{f}{f+2KV}\frac{\partial V_g}{\partial z} - \frac{V^2}{f+2KV}\frac{\partial K}{\partial z}. \tag{5}$$

The second term on the right can hardly be evaluated from the available data. Assuming the radius of curvature to differ by the fairly large amount of 200 km through the depth of the front, this term would amount to about $2 \times 10^{-3}\,\mathrm{sec}^{-1}$ or only about 6 per cent of the observed shear. Utilizing only the first term on the right of eq. (5), the radius of curvature is computed to be 1350 km, which agrees closely with the curvature measured from the maps. Thus the curvature adequately accounts for the ratio of about two, between the observed and geostrophic vertical shears within the frontal layer.

A further example of the appreciable dif-

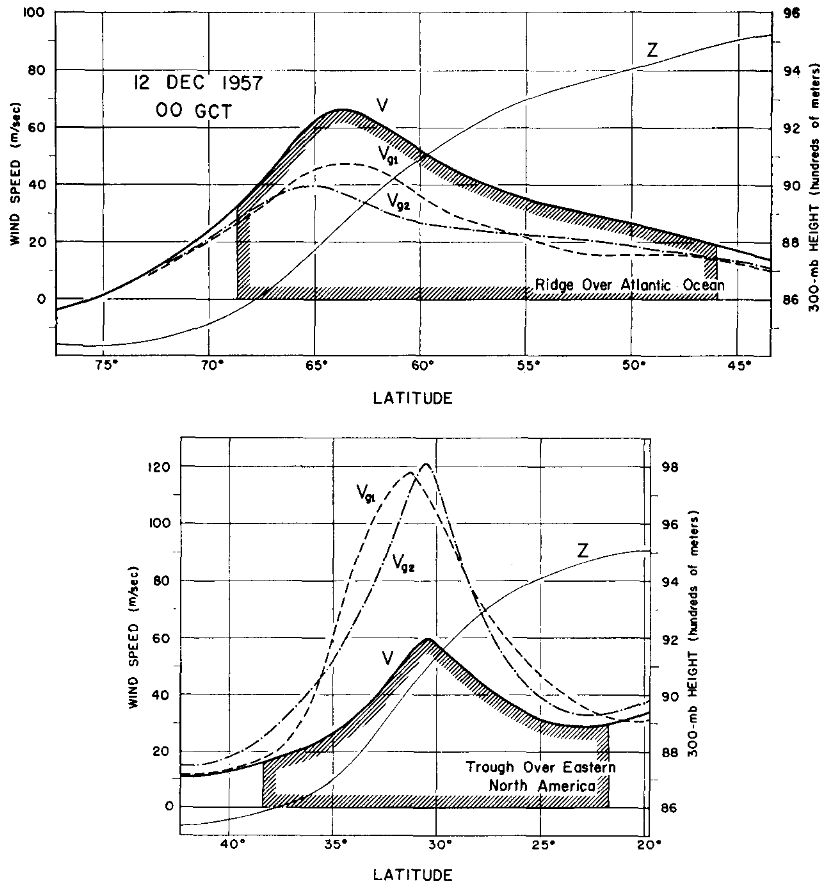

Fig. 7. Profiles of 300-mb height (Z) and wind speed (V) along ridge and trough lines. V_{g1} and V_{g2} are geostrophic wind profiles (see text).

ference between the vertical shear and the geostrophic thermal shear is evident from Fig. 5*a*. The influence of curvature on the vertical shear and frontal slope in the troposphere has already been mentioned. Above the jet stream, a strong thermal shear is apparent, but the decrease of wind with height is relatively weak.

Between Montgomery (226) and Tampa (211) in Fig. 5*a*, the mean geostrophic wind decreased upward by about 64 m/sec between the 300-mb and 100-mb levels. The only wind sounding reaching high levels in this region was Valparaiso (221), which showed a wind speed decrease of only 15 m/sec through this layer. In eq. (5), the quantity 2KV in the denominator was almost equal to $2f$, the wind difference from 300 to 100 mb computed from the first term on the right being -23.5 m/sec. The radius of curvature at 100 mb was about 200 km greater than at 300 mb, the contribution from the second term being $+3.5$ m/sec.

The total wind difference of -20 m/sec from 300 to 100 mb, computed from eq. (5), compares fairly well with the observed wind decrease of -15 m/sec at Valparaiso. Although this single observation is not necessarily representative of the mean conditions in the vicinity of the trough, this example again illustrates the great difference (in this case, by more than a factor of three) which may obtain between the actual vertical shear and the geostrophic thermal shear.

6. Fields of divergence and vertical velocity

The vertical velocity in the eastern part of the United States was computed from the kine-

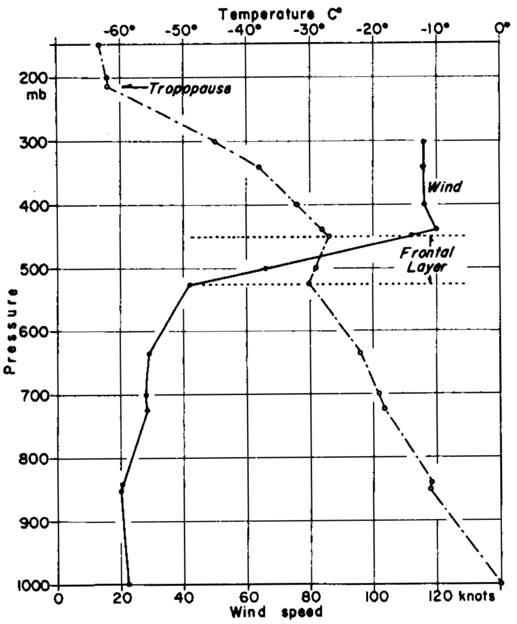

FIG. 8. Profiles of wind speed and temperature at Ship "A" (see location on Fig. 3).

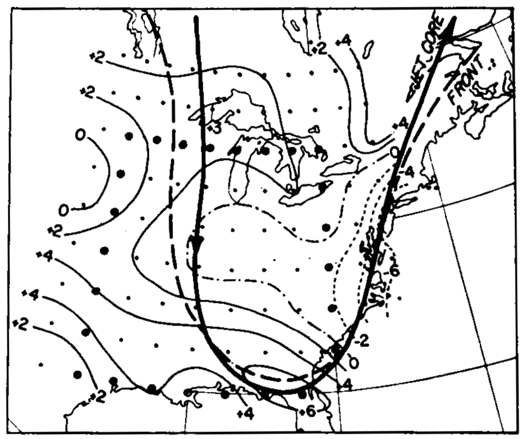

FIG. 9. Vertical velocity (microbars per second) at 500–mb surface. Positive values (solid isopleths) correspond to air motions downward through isobaric surface.

matically determined wind divergence in grid points 2.5 degrees of latitude and longitude apart. Fig. 9 shows the distribution of ω in microbars per second (μb/sec) at the 500-mb surface. The 500-mb frontal contour and the 300-mb jet axis are also indicated. Except for a relatively small region in the central parts of the cold upper trough where weak ascending motion can be observed, and a belt along the front at the east coast where strong ascending motion prevails, the region as a whole is characterized by descending motion. Especially strong is the descending motion in the southern parts of the United States.

The mean divergence and vertical velocity for 56 grid points in the region outlined in Fig. 9 are given in Fig. 10. From this it can be seen that, on the average, divergence prevailed up to about 600 mb with convergence above 400 mb. The vertical velocity increased with height to about 600 mb and remained almost constant up to 400 mb, decreasing above that level. Around the 500-mb level, $\bar{\omega}$ reached values of about 1.8 μb/sec, corresponding to a velocity of about −2.6 cm/sec.

The distribution of vertical velocity is shown in Fig. 11, in a vertical section corresponding to Fig. 4 (line I–I on Fig. 3). On the whole, descending motions are indicated in the warm air on the west side of the upper trough, and ascending motions on the east side. The latter reach maximum values of about 10 cm/sec in the region of the cyclone developing near the East Coast (Fig. 1).

Superimposed on this overall pattern, vertical motions of the opposite sort are seen within the polar air, with ascent west and descent east of the trough line. The type of vertical circulation shown in Fig. 11 is equivalent to conversion of kinetic energy into potential energy to the west, and conversion of potential energy into kinetic energy in the east where warm air rises and cold air sinks. This distribution of vertical velocities

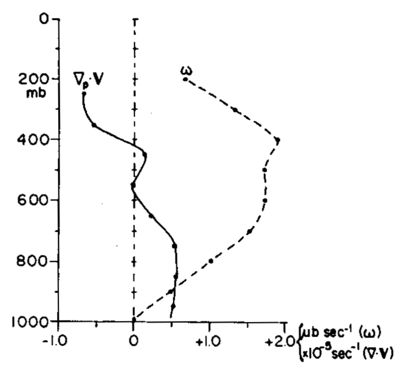

FIG. 10. Divergence and vertical velocity, averaged over region bounded by and including encircled points in Fig. 9.

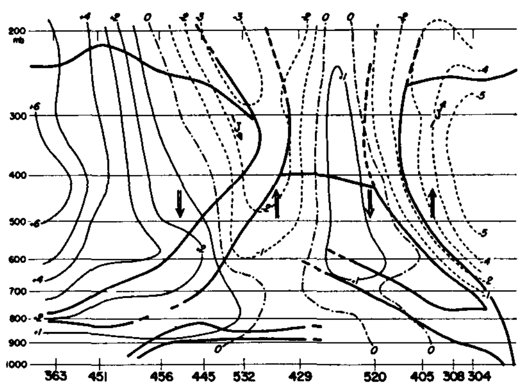

FIG. 11. Vertical velocity (μb/sec) in cross section I (corresponding to Fig. 4).

and energy conversion seems to be in at least qualitative agreement with the deceleration of the jet on the west side and acceleration on the east side of the trough, which can be seen from the 300-mb isotach pattern in Fig. 12.

The geostrophic deviations discussed earlier (Fig. 7) are a direct expression of the centripetal accelerations. A basic problem in understanding the dynamics of wave patterns is to account for the appreciable difference in baroclinity between troughs and ridges, which is required to account for the centripetal accelerations. In an earlier study, PALMÉN and NAGLER (1949) deduced that the thermal gradient in troughs must be stronger than that which would be produced by horizontal confluent motions alone, upstream from the trough. They concluded that the warm air approaching a trough line must descend relative to the cold air, with the opposite on the east side of the trough, as indicated by the vertical arrows in Fig. 11. The process they suggested is substantiated by the computed vertical motions shown here. Differential adiabatic heating and cooling contribute to intensify the thermal gradient in air approaching the trough, and to weaken it in air leaving the trough.

Of special interest is the behavior of the jet stream. In Fig. 13 the core of the jet is marked by a heavy line, and the thinner lines show the distribution of divergence at about 250 mb (taken as the mean value between 300 and 200 mb, to minimize the errors in computation at individual levels). The jet core seems to mark the regions of strongest positive or negative divergence. Appreciable divergence prevails in the northwestern part, and strong convergence in

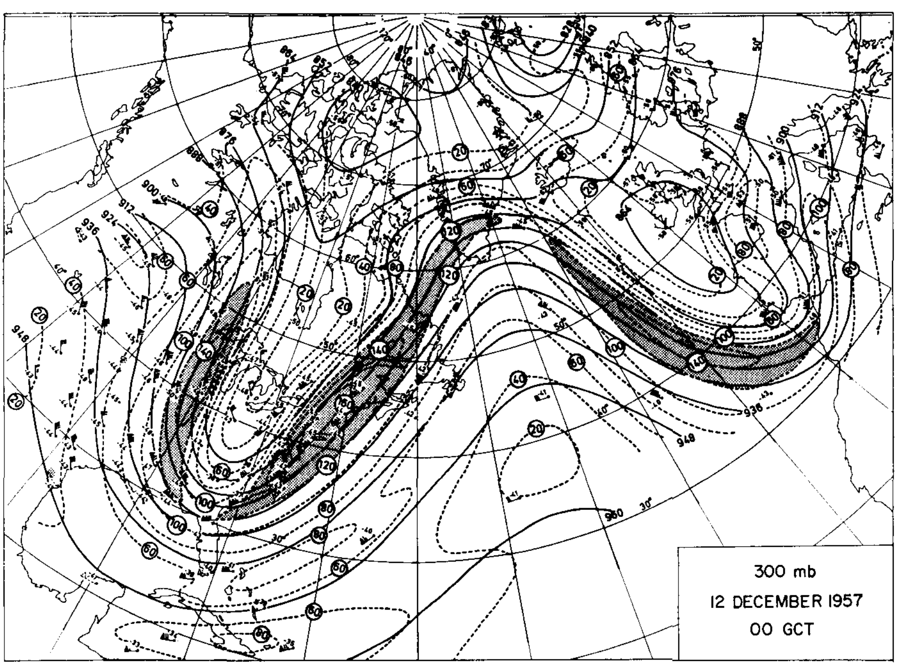

FIG. 12. 300-mb chart, 00 GMT December 12, 1957. Solid lines, contours (tens of meters), dashed lines, isotachs (stippled areas, wind speed in excess of 120 knots). Temperatures plotted to left of stations.

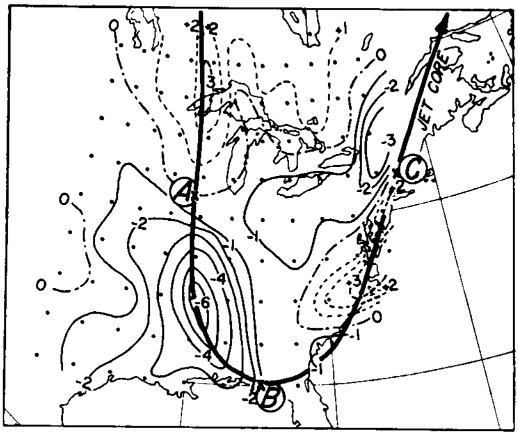

FIG. 13. Mean divergence (computed from observed winds) in 200–300 mb layer. Units are 10^{-5}sec^{-1}.

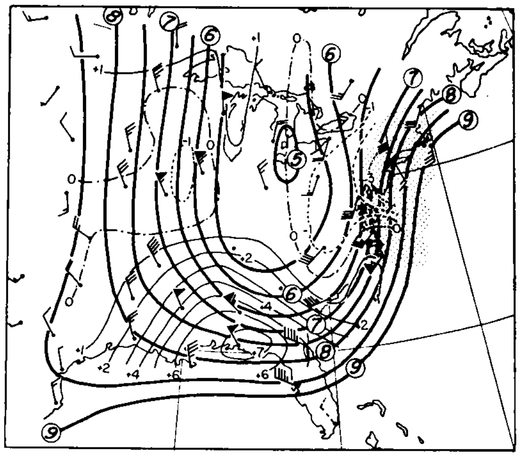

FIG. 14. Pressure in decibar of the 285°K isentropic surface (heavy lines), and winds and instantaneous vertical motions (thin lines, μb/sec) at that surface, 00 GMT December 12, 1957.

the southwestern parts. On the east side again, divergence marks the jet core in the region of the wave cyclone, whereas convergence occurs farther northwards. From the vorticity equation in the form

$$\frac{d\eta}{dt} = -\eta\nabla\cdot\mathbf{V}, \tag{6}$$

we get
$$\eta_1 - \eta_0 \approx -\bar{\eta}\,\overline{\nabla\cdot\mathbf{V}}\,(t_1 - t_0), \tag{7}$$

where $\eta_1 - \eta_0$ is the change of absolute vorticity following an individual particle during the time $t_1 - t_0$, and $\bar{\eta}$ and $\overline{\nabla\cdot\mathbf{V}}$ denote mean values during the same time. From this equation a crude estimate of the change of vorticity along the jet core can be made, under the assumption that an air particle remains in the axis of the jet stream where shear is absent.

According to this estimate the vorticity should decrease on the west side of the trough down to latitude 41°, increasing south of this latitude. The maximum vorticity should appear southeast of the trough, whereas a decrease again should occur northwards to about latitude 42°N on the East Coast. In the jet core the absolute vorticity is

$$\eta = K_s V + f, \tag{8}$$

where K_s is approximated by the curvature of the jet.

The change of absolute vorticity from point A to point B in Fig. 13 amounts to $+0.7 \times 10^{-4}$ sec^{-1} and from point B to point C it amounts to $-0.9 \times 10^{-4}\text{sec}^{-1}$. An air parcel in the jet core needs about 2.1×10^4sec to travel between these points, at the mean velocity in the jet core. If we assume a mean vorticity of $1.35 \times 10^{-4}\text{sec}^{-1}$ between A and B, and 1.25×10^{-4} sec^{-1} between B and C, the mean divergence required to act on the parcels would be $-2.5 \times 10^{-5}\text{sec}^{-1}$ and $+3.5 \times 10^{-5}\text{sec}^{-1}$ respectively. The former value is in good agreement with the mean convergence according to Fig. 13, but the latter is considerably larger than the mean divergence on the map. It should, however, be noted that the eastern divergence field is at the boundary of our area of computation and is therefore less reliable. As a whole, however, the vorticity distribution along the jet core is in sufficiently good agreement with the computed divergence field.

The field of motion and the isobaric contours at the isentropic surface 285°K are shown in Fig. 14. This surface reaches the upper troposphere (about 500 mb) in the central part of the cold dome, and coincides nearly with the lower boundary of the polar front in the lower troposphere (cf. Fig. 4b.). Vertical motions shown on this chart were computed from the adiabatic relationship

$$\omega = (V - C_s)\left(\frac{\partial p}{\partial s}\right)_\theta. \tag{9}$$

The speed of movement C_s of an isentropic contour along the direction of a streamline was determined from successive maps at 12-hr intervals, with contours interpolated according to continuity principles at 6-hr or shorter intervals where necessary to give a reasonably accurate estimate of the movement.

The principal feature of the vertical motion field is strong subsidence in the southern part of the cold trough, this being most pronounced beneath the jet stream somewhat west of the upper trough line. The maximum descent, at about the 750-mb level, is of about the same strength as the maximum descent at 500 mb, computed by the kinematic method (Fig. 9). In the portion of the cold tongue farther north, generally weak descent is indicated, except for a small region of weak ascending motions west of the trough and stronger ascent associated with the surface cyclone, near the East Coast.

The field of vertical motion shown in Fig. 14 is very similar to that found in an earlier study of a major cold outbreak, by PALMÉN and NEWTON (1951). The same is true of the pattern of isentropic trajectories (not shown). During the 24-hr period ending at the time of Fig. 14, a family of trajectories originating on the west side of the cold tongue showed a pronounced lateral spreading, the character of which is well indicated by the wind observations. Trajectories originating near 600 mb SW of Lake Michigan curved cyclonically, ending NW of Hatteras after a slight descent followed by ascent in passing through the central portion of the cold tongue where vertical motions were weak. Others, originating also near 600 mb farther northwest and located in the belt of strongest winds, moved from the Canadian border to the central Gulf of Mexico coast in 24 hr. These showed first a weak then a more rapid descent, amounting to 200–220 mb in this period. Their curvature was at first slightly cyclonic, changing to anticyclonic near the Gulf Coast, reflecting vertical shrinking in the area of strong general subsidence in the southern portion of the cold dome.

7. Divergence on scale of long wave

It is of interest to compare the divergence values in Fig. 13 with the divergence on the long-wave scale. The mean divergence may be computed from the relationship

$$\bar{D} = \frac{1}{A} \oint V_n \delta l, \tag{10}$$

where A is the area inside an arbitrarily selected boundary, of which δl is a length element, and V_n is the outward-directed component of velocity normal to the boundary. It is convenient to make this computation for the 300-mb level between the major trough over eastern North America and the ridge over the Atlantic Ocean. As the lateral boundaries, the 8560-m and 9480-m contours are chosen, which include the most significant part of the flow (Fig. 12).

The areas inside the hachures in the upper and lower parts of Fig. 7 measure the export $\int V_n \delta l$ through the eastern boundary, and the import through the western boundary, of this region. These are found to be, respectively, 105×10^6 and $67 \times 10^6 \mathrm{m^2 sec^{-1}}$. The flow of air across the southern and northern boundaries cannot be evaluated directly from the winds, because it is sensitive to small angular deviations between winds and contours. The average value of v_n (in this expression, the component of wind toward lower contours) may be approximated from the relation

$$f v_n = \frac{dV}{dt} \approx \frac{\partial V}{\partial t} + v_n \frac{\partial V}{\partial n} + V \frac{\partial V}{\partial l},$$

or $$v_n = \left(\frac{\partial V}{\partial t} + V \frac{\partial V}{\partial l}\right)\left(f - \frac{\partial V}{\partial n}\right)^{-1}.$$

Here the vertical transport term $w \partial V / \partial z$, which is probably small at 300 mb on the average but cannot be evaluated, has been omitted.

Mean values of V, $\partial V/\partial l$ and $\partial V/\partial n$ may be taken directly from Fig. 12, while $\partial V/\partial t$ can be estimated from successive maps. Within the range (owing to sparsity of observations) of reasonable estimates of $\partial V/\partial t$, $\bar{v}_n$ for the southern contour was found to be between -0.8 and $+0.8$ m/sec, and for the northern contour between -0.9 and -1.4 m/sec. These values correspond to an import or export of $4 \times 10^6 \mathrm{m^2 sec^{-1}}$ across the southern contour, and an import of 4 to $7 \times 10^6 \mathrm{m^2 sec^{-1}}$ across the northern contour.

From the above values, the total export from the chosen region is found to be $(32 \pm 5) \times 10^6$ $\mathrm{m^2 sec^{-1}}$. Inserting this, along with the area A ($9.4 \times 10^{12} \mathrm{m^2}$), into eq. (10), we find that

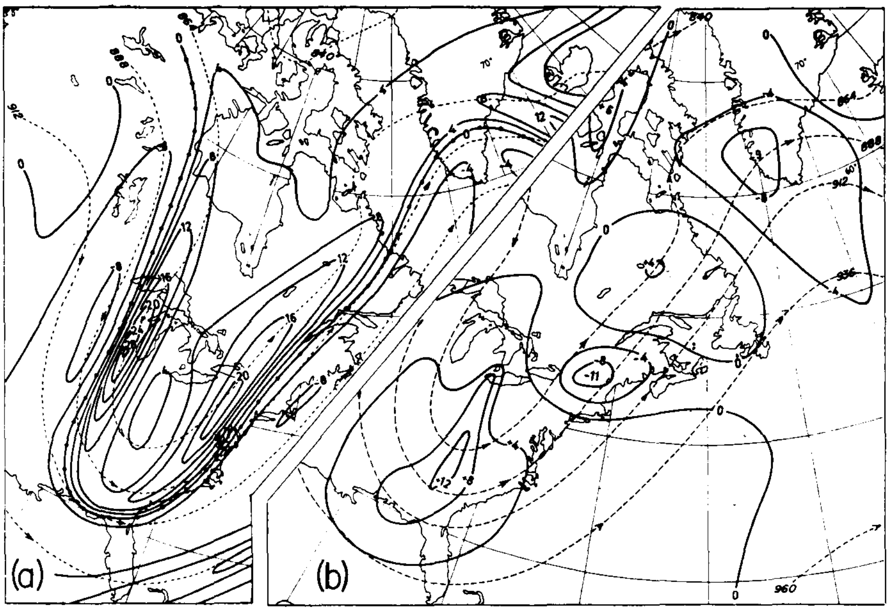

FIG. 15. Relative vorticity due to shear (*a*) and curvature (*b*) at 300 mb, corresponding to map in Fig. 12. Units are 10^{-5}sec^{-1}. Dashed lines, isobaric contours.

$$\overline{D} = (3.4 \pm 0.5) \times 10^{-6}\text{sec}^{-1}.$$

Thus the mean divergence, on the scale of the long wave, is an order of magnitude smaller than the largest values of divergence (Fig. 13) associated with the cyclone-scale disturbances. Appreciable values of the latter are found in only small regions, compared with the area considered above. Owing to this, and to the presence of alternating regions of divergence and convergence between long-wave trough and ridge, their individual influences tend to cancel and the mean divergence over a larger region is left as a small residual. This distinction between cyclone-scale disturbances and long waves is already well known, but the above comparison of numerical values serves to emphasize it.

8. Real and geostrophic vorticity fields at 300 mb

The vorticity of the actual wind field was computed from analyses of the isotachs and isogons at the 300-mb level. Isotachs (Fig. 12) were based on observed winds, supplemented by geostrophic winds where the streamlines were straight. At several stations near the jet stream, extrapolations of the velocity profiles in observations reaching above the 400-mb level were utilized, taking into account the thermal fields and the wind variations with height at neighboring stations.

The analysis of isotachs, streamlines and isogons was done with the greatest possible care, having regard for consistency between the normal and tangential accelerations implied by this analysis, and the height gradients. Thus although there are appreciable regions without direct wind observations, the wind analyses are as closely as possible compatible with the contour field. Curvatures, computed from the isogon analyses by use of eq. (3), differ appreciably from contour curvatures in some regions. For example, in the neighborhood of the trough over the southeastern United States where there is deceleration upstream and acceleration downstream, the streamline curvature is considerably sharper than the contour curvature.

Absolute vorticity was computed from the expression

$$\eta = f + \frac{\partial V}{\partial n} + V\frac{\partial \beta}{\partial s} + \frac{u}{a}\tan\Phi. \qquad (11)$$

Here V is the total wind speed, n is positive toward right of the wind, β is the wind direction

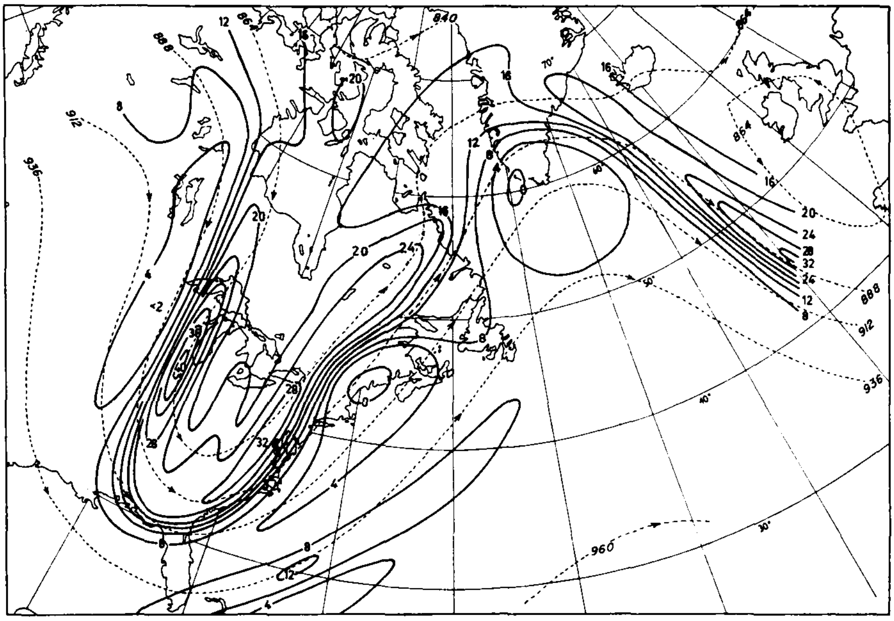

FIG. 16. Absolute vorticity, corresponding to Fig. 15.

measured positive counterclockwise from east, u is the eastward component, and a is the radius of the earth. Measurements of the direction and speed gradients were made at a large number of points, differentials being taken generally over distances of 100–200 km. At certain lines across the current, speed profiles were plotted and shears measured from their slopes, to minimize errors due to finite-difference measurements.

The horizontal shear $\partial V/\partial n$ is shown in Fig. 15*a*. As would be expected, shears are strongest on the flanks of the wind-speed maxima (Fig. 12), which are located near the inflections of the large-scale wave pattern. The contribution of curvature (last two terms on right of eq. 11) is shown in Fig. 15*b*.

Fig. 16 shows the field of absolute vorticity, which is strongly dominated by the shear. The appreciable distortion in the neighborhood of New England (compare Fig. 15) results from a weak anticyclonic curvature in this region, in combination with strong wind speeds. This curvature is not evident from the contour field, being associated with cross-contour flow components upstream and downstream from the wind-speed maximum in this locality.

The pattern of absolute vorticity of the wind field in Fig. 16 may be compared with that of the geostrophic absolute vorticity, $f + gf^{-1}\nabla^2 z$, shown in Fig. 17. The Laplacian was computed with use of a grid having arms of length 300 km (true at latitude 45°, variations of map scale being taken into account). Computations were made at locations chosen to bring out the maximum and minimum values.

The field of geostrophic vorticity differs considerably from that of the real vorticity, as shown by the differences mapped in Fig. 18. In the major trough, a large overestimate of vorticity north of the jet, and the negative values to the south, result from the great differences between geostrophic and real wind speed where the wind is strong, this difference being smaller where the wind is weak (compare slopes of V and V_g profiles in Fig. 7). Minimization of the strong shears near the inflections (Fig. 15*a*) is due to truncation error, the double grid length being greater in some places than the distance between the maximum and minimum shear values. The minimum of vorticity near New England (Fig. 16), associated with small curvatures due to the ageostrophic wind components, vir-

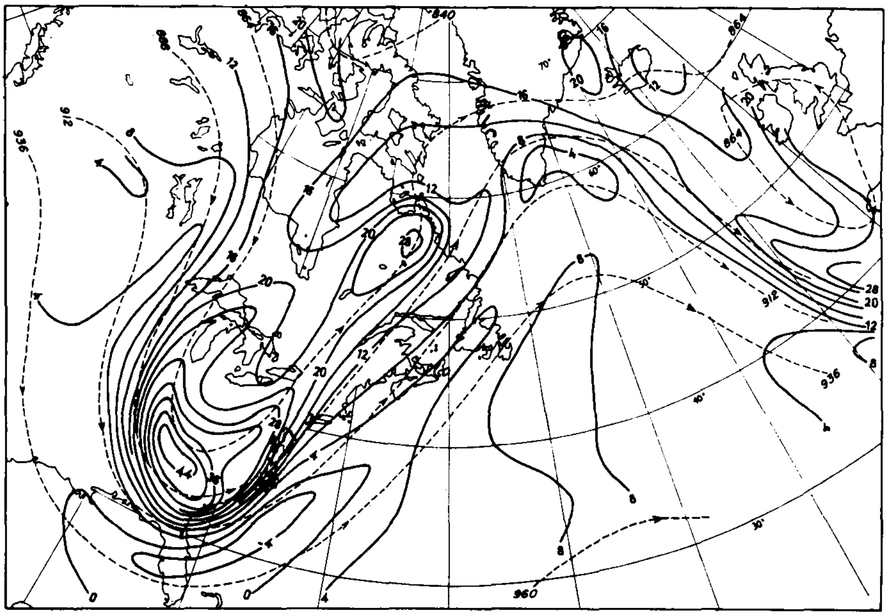

FIG. 17. Geostrophic absolute vorticity computed from map in Fig. 12.

tually disappears in the geostrophic vorticity field.[1]

Comparison with Fig. 1 suggests that Fig. 16 provides a much more adequate notion of the vorticity advection, and thus of the divergence field judged from it, than does the geostrophic vorticity field in Fig. 17. The two principal regions where the vorticity decreases downstream correspond fairly well with the deep cyclone over northern Labrador and the cyclone northeast of Hatteras, in which the central pressure fell 16 mb during the 24 hr centered on map time.

9. Systematic cross-contour meandering associated with vertical motions in middle troposphere

The most readily recognized type of departure from gradient flow is that associated with horizontal variations of wind speed along the current, as typified by the velocity distribution in Fig. 12. DURST and SUTCLIFFE (1938) showed that significant cross-isobar flow may also occur in association with organized vertical motions. In the simplest case, supposing that there is geostrophic balance at the level of origin of an air parcel, its ascent or descent in a baroclinic field will carry it to levels where the horizontal pressure gradient is stronger or weaker, and lateral motion across the isobars results from the imbalance created between coriolis and pressure-gradient forces. In a study based directly on the wind field, GODSON (1950) demonstrated that, at the 700-mb level, the convective accelerations associated with vertical motions are of the same order of magnitude as those associated with horizontal variations of wind velocity.

In the following discussion, an attempt will be made to evaluate the influence of vertical motion on the trajectories followed by air parcels travelling through a wave system. In the interest of simplicity and in order to isolate this influence from others which may also be present in a real situation, a very simple wave structure will be assumed. This is a sinusoidal wave (Fig. 19) in which the wind speed varies with height according to the relationship

$$V = V_0 + Sz, \qquad (12)$$

[1] It should be noted that some of the differences noted above would be partially alleviated when the vorticity is computed by use of the balance equation, as is the practice in analysis by electronic computer methods.

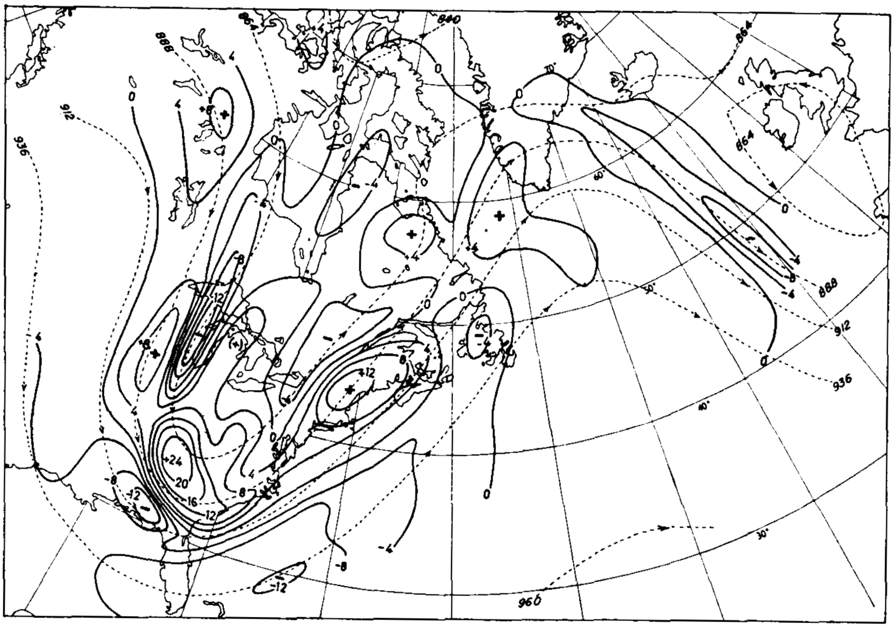

FIG. 18. Geostrophic vorticity minus vorticity of the real wind field.

where $S \equiv \partial V/\partial z$ is taken as positive in the troposphere. The wave system is assumed stationary, a trajectory being identical with a streamline. The wind speed is allowed to vary across, but not along, the direction of the contours at a given isobaric surface.

If V_i is the component of wind parallel to an isobaric contour and v_n the cross-contour component toward lower geopotential, $dV_i/dt = fv_n$.

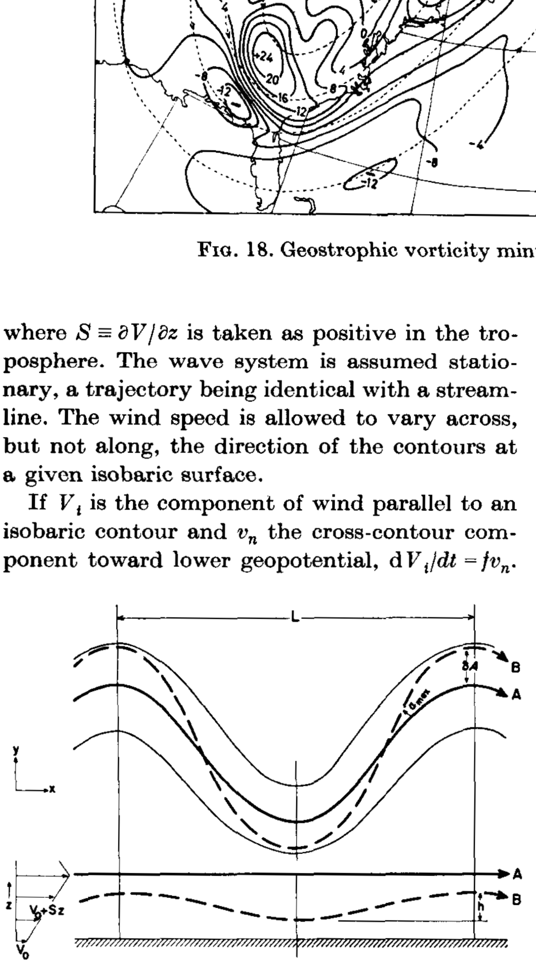

FIG. 19. Simplified wave pattern showing streamline (A) parallel to isobaric contours at an upper level, and the modification (streamline B) associated with vertical motion (see text). In lower part, projections of streamlines A and B on a vertical section; at left, variation of wind speed with height.

When the wind direction does not deviate greatly from that of the contours, V_i closely approximates the total wind speed and $dV/dt \approx fv_n$. Letting i denote distance along an isobaric contour and n distance normal to it, expansion of this expression gives, after rearrangement of terms,

$$v_n \approx \left(\frac{\partial V}{\partial t} + V\frac{\partial V}{\partial i} + w\frac{\partial V}{\partial z}\right)\left(f - \frac{\partial V}{\partial n}\right)^{-1}. \qquad (13)$$

Under the assumptions stated above, the first two terms in the first parentheses drop out and, on substitution from eq. (12),

$$v_n \approx \frac{wS}{\Sigma}, \qquad (14)$$

where $\Sigma \equiv (f - \partial V/\partial n)$.

Since the angle of cross-contour flow is given by $\alpha \approx v_n/V$, it follows from eq. (14) that

$$\alpha \approx wS/V\Sigma. \qquad (15)$$

Normally $\Sigma > 0$ and a sinusoidal wave is characterized by overall descending motions upstream from and ascending motions downstream from a trough. For an air particle in the middle troposphere, eq. (15) then implies a meandering such as is described by the three-dimensional trajectory "B" in Fig. 19, while particle "A", taken to be at the level of maximum wind where shear is absent, would follow a contour.

If $S = 5 \times 10^{-3}\text{sec}^{-1}$, $V = 30$ m/sec, and $\Sigma = 0.5 \times 10^{-4}\text{sec}^{-1}$ ($f = 10^{-4}\text{sec}^{-1}$, $\Sigma = 0.5f$), eq. (15) gives a value for α of 1/3 radian or 19°, if w is as large as 10 cm/sec. Vertical motions of this size are characteristic of cyclone-scale disturbances, but mean values of divergence and vertical motion are much weaker on the long-wave scale. Hence the cross-contour flow pertaining to the latter scale would be very small and impossible to detect with ordinary types of observations.

The magnitude of the overall cross-contour meandering of an air particle while moving from trough to ridge of a long wave may, however be estimated. In Fig. 19, let δA be the difference between the amplitudes of trajectories "B" and "A". While going from trough to ridge in time Δt, particle "B" would undergo a total cross-contour movement $2\delta A$ and a total vertical movement h. From eq. (14),

$$2\delta A \approx \int_{\Delta t} v_n dt = \int_{\Delta t} \frac{wS}{\Sigma} dt = \frac{hS}{\Sigma}. \qquad (16)$$

Using the values of S and Σ mentioned earlier, and adopting a value of 3 km for the vertical movement[1] h,

$$2\delta A \approx 300 \text{ km}.$$

From eq. (15), it is evident that if the vertical motion has a sinusoidal variation along the current with maximum values at the inflections, trajectory "B" will be a sine wave in phase with "A". For a sinusoidal wave, the curvature at the troughs and ridges (see, e.g. Bjerknes and Holmboe, 1944) is

$$K = \pm \frac{4\pi^2}{L^2} A, \qquad (17)$$

where A is the amplitude and L the wavelength. Referring to Fig. 19, the difference in curvature of trajectories "B" and "A" is

$$\delta K = \pm \frac{4\pi^2}{L^2} \delta A \approx \pm \frac{2\pi^2}{L^2} \frac{hS}{\Sigma}, \qquad (18)$$

where the upper sign applies at the trough. Using the values mentioned earlier, and taking $L = 6000$ km,

$$\delta K \approx \pm 16.5 \times 10^{-8} \text{m}^{-1}. \qquad (19)$$

The above treatment, which is intended only to arrive at an order-of-magnitude estimate of the meandering connected with vertical motions, is obviously oversimplified. The chosen values of S and Σ correspond to approximate means throughout the troposphere, a few hundred km to the right of the jet stream. It may be noted that when values representative of the frontal layer near 500 mb are inserted into eq. (18), a value for δK is obtained which is about 1.5 times that indicated above.

In eq. (13), the first and third terms within the first parentheses normally have the same sign, on the anticyclonic-shear side of the jet stream when the wave system is progressive. Thus in that zone, the ensuing equations would give an underestimate of the cross-contour meander in the middle troposphere. According to Godson's (1950) findings, $\partial V/\partial t$ was of the same order as, and averaged somewhat smaller than, $w\partial V/\partial z$ at the 700-mb level.

10. Influence of curvature variations on the vertical shear relationship

Although the curvature difference δK in eq. (19) may seem rather small, it is large enough to be significant in the relationship between the vertical shear and the solenoid field, when the anticyclonic curvature and shear are large. To demonstrate this, we may examine the wind observation at Ship "A" (Fig. 8).

At 300 mb, $V = 59$ m/sec and $V_g = 36$ m/sec (taking the average of V_{g1} and V_{g2} from Fig. 7). From eq. (1), $K = -8.6 \times 10^{-7}$ m^{-1}, corresponding to a trajectory radius of 1160 km. The value of δK in eq. (19), if applied to the tropospheric layer above the front, would corresond to a difference of about 220 km, between the radii of curvatures at the 450-mb and 300-mb levels.

[1] In Section 4, the mean divergence between long-wave trough and ridge was found to be 3.4×10^{-6} sec^{-1} at 300 mb, corresponding to a mean upward motion in the middle troposphere of about 1 cm/sec if a typical divergence variation with height is assumed. Since this applies to a region about 2200 km wide, a value of $\bar{w} = 2$ cm/sec near the jet stream does not seem excessive. In the wave of Fig. 3, an air particle travelling at 30 m/sec would require about 1.5 days to go from trough to ridge, with a total vertical displacement of the order of 3 km.

With the computed curvature, the ratio $f/(f+2KV)$ in eq. (5) is 4.5. From Fig. 6*a*, the horizontal temperature gradient is estimated to be 3°C in 500 km, and $\partial V_g/\partial z = +1.9 \times 10^{-3}$ sec^{-1}.

The vertical shear computed only from the first term on the right of eq. (5) would be $+8.5 \times 10^{-3} \text{sec}^{-1}$. The observed shear was actually nil (or perhaps slightly negative).

The requirement for the vertical shear to vanish is, from eq. (5), that

$$\frac{\partial K}{\partial z} = \frac{f}{V^2}\frac{\partial V_g}{\partial z}.$$

Inserting the values mentioned above, the value of $\partial K/\partial z$ required for the shear to vanish is found to be $+7.1 \times 10^{-11} \text{m}^{-2}$, corresponding to a value of $\delta K = 20.6 \times 10^{-8} \text{m}^{-1}$ for the difference of curvature through the layer. With the available observations, it is not possible to verify this value directly. However, the fairly close agreement with the value in eq. (19) suggests that the influence on curvature, which arises from the presence of vertical motion in the middle troposphere, is of the right order of magnitude to account for the observed vertical shear. The closeness of agreement is considered fortuitous, in view of the several approximations involved.

It appears safe to make the generalization that, since baroclinity is generally present and this would otherwise imply very large vertical shear when strong anticyclonic curvature is present, variation of curvature with height of the kind described by Fig. 19 is an essential feature of wave structures.

[1] The importance of low dynamic stability in relation to lateral upglide motions in frontal layers has been stressed by BJERKNES (1951). The present discussion is, while treating different aspects, closely related to his treatment.

The reader will note from Fig. 6*a* that although the vertical shear was small south of the jet stream, it was large (about 10 m/sec per km) above the frontal layer, north of the jet axis. Although the observations are inadequate to examine the situation quantitatively, it may be pointed out that there are fundamental differences between the cyclonic-shear and the anticyclonic-shear sides of the jet stream, from the point of view of the above discussion. Within the upper part of the frontal layer, the vertical shear is smaller relative to the horizontal shear; thus the ratio S/Σ in eq. (14) is smaller.[1] Also, referring to Fig. 11, vertical motions are likely to be greater on the anticyclonic side. With a progressive wave, $\partial V/\partial t$ in eq. (13) contributes to diminish v_n on the cyclonic-shear side, and to augment v_n on the anticyclonic flank of the jet stream. Consequently the type of middle-tropospheric meandering described by Fig. 19, which contributes to diminish the vertical shear in the ridge, may be expected to be damped on the cyclonic-shear side of the jet stream.

Acknowledgements

The research reported in this paper was made possible through partial support by and use of facilities of the Institute of Meteorology, University of Stockholm, and of the Department of the Geophysical Sciences, University of Chicago. We wish to thank Professor B. Bolin and Professor S. Petterssen for their kindness in arranging for us to collaborate at these institutions. This collaboration was further enabled by the U.S. Weather Bureau, through the assignment of one of us (C. W. Newton) to the University of Stockholm in Autumn 1961, and the arrangement for the other (E. Palmén) to work in Kansas City in Autumn 1962.

REFERENCES

BJERKNES, J., 1937, Theorie der aussertropischen Zyklonenbildung. *Meteor. Zeits.*, 54, pp. 462–466.

BJERKNES, J., 1951, Extratropical cyclones. In *Compendium of Meteorology* (T. F. Malone, Ed.). Boston, Amer. Meteor. Soc., pp. 577–598.

BJERKNES, J., and HOLMBOE, J., 1944, On the theory of cyclones. *J. Meteor.*, 1, pp. 1–22.

BRADBURY, D., and PALMÉN, E., 1953, On the existence of a polar-front zone at the 500-mb level. *Bull. Amer. Meteor. Soc.*, 34, pp. 56–62.

DURST, C. S., and SUTCLIFFE, R. C., 1938, The importance of vertical motion in the development of tropical revolving storms. *Quart. J. R. Meteor. Soc.*, 64, pp. 75–84.

EXNER, F. M., 1925, *Dynamische Meteorologie*. Verlag Julius Springer, Vienna.

FLEAGLE, R. G., 1947, The fields of temperature, pressure and three-dimensional motion in selected weather situations. *J. Meteor.*, 4, pp. 161–185.

FORSYTHE, G. E., 1945, A generalization of the thermal wind equation for arbitrary horizontal flow. *Bull. Amer. Meteor. Soc.*, 26, pp. 371–375.

GODSON, W. L., 1950, A study of the deviation of wind speeds and directions from geostrophic values. *Quart. J. Roy. Meteor. Soc.*, **76**, pp. 3–15.

NEWTON, C. W., and PERSSON, A. V., 1962, Structural characteristics of the subtropical jet stream and certain lower-stratospheric wind systems. *Tellus*, **14**, pp. 221–241.

PALMÉN, E., 1951*a*, The role of atmospheric disturbances in the general circulation. *Quart. J. R. Meteor. Soc.*, **77**, pp. 337–354.

PALMÉN, E., 1951*b*, Aerology of extratropical disturbances. In *Compendium of Meteorology* (T. F. Malone, Ed.). Amer. Meteor. Soc., Boston, pp. 599–620.

PALMÉN, E., 1958, Vertical circulation and release of kinetic energy during the development of Hurricane Hazel into an extratropical storm. *Tellus*, **10**, pp. 1–23.

PALMÉN, E., and NAGLER, K. M., 1949, The formation and structure of a large-scale disturbance in the westerlies. *J. Meteor.*, **6**, pp. 227–242.

PALMÉN, E., and NEWTON, C. W., 1951, On the three-dimensional motions in an outbreak of polar air. *J. Meteor.*, **8**, pp. 25–39.

PETTERSSEN, S., 1955, A general survey of factors influencing development at sea level. *J. Meteor.*, **12**, pp. 36–42.

PLATZMAN, G. W., 1947, Some remarks on the measurement of curvature and vorticity. *J. Meteor.*, **4**, pp. 58–62.

RIEHL, H., ALAKA, M. A., JORDAN, C. L., and RENARD, R. J., 1954, The jet stream. *Meteor. Monographs*, v. **2**, No. 7, 100 pp.

ROSSBY, C.-G., 1942, *Kinematic and hydrostatic properties of certain long waves in the westerlies.* Univ. Chicago, Dept. of Meteor., Misc. Reps. No. 5.

SUTCLIFFE, R. C., 1947, A contribution to the problem of development. *Quart. J. R. Meteor. Soc.*, **73**, pp. 370–383.